Effects of Manufacturing Tolerances on Double Wall Effusion Cooling

Michael van de Noort*[1], Peter T. Ireland[1] and Janendra C. Telisinghe[2]

[1] Dept. of Engineering Science, University of Oxford

Oxford, OX1 3PJ, United Kingdom

Email: michael.vandenoort@eng.ox.ac.uk, peter.ireland@eng.ox.ac.uk

[2] Turbines, Rolls-Royce PLC.

Bristol, BS34 7QE, United Kingdom

Email: janendra.telisinghe@rolls-royce.com

Abstract

As aeroengine designers seek to raise Turbine Entry Temperatures for greater thermal efficiencies, novel cooling schemes are required to ensure that components can survive in increasingly hotter environments. By utilising a combination of impingement cooling, pin-fin cooling and effusion cooling, Double-Wall Effusion Cooling is well equipped to achieve the high metal cooling effectiveness required for such challenges whilst keeping coolant consumption at an acceptably low level. However, this high performance can drop-off within the variability of common manufacturing tolerances, which can also expose cooling schemes to issues such as hot gas ingestion.

This paper uses an experimentally validated Low Order Flow Network Model (LOM) to assess the cooling performance of a Double Wall Effusion Cooling scheme employed in a High Pressure Turbine Nozzle Guide Vane, subject to the variability of geometric parameters set by their manufacturing tolerances. The relative significance of each geometric parameter is examined by varying it individually and comparing the effects on the cooling performance. A Monte Carlo analysis is then conducted to assess the likelihood of performance variation for a baseline design. Finally, multiple optimisation studies are conducted for the cooling scheme, with the simultaneous objectives of reducing coolant usage and maximising the design tolerances to reduce manufacturing cost, all whilst maintaining acceptable metal cooling effectiveness and backflow margins.

Keywords: Flow Networks, Coolant Migration, Double-Wall Effusion Cooling, Quasi-Transpiration Cooling

1 Introduction

The need to increase Turbine Entry Temperatures to increase turbine thermal efficiencies has been a hot topic in modern aeroengine design for some time. The use of such TETs exposes turbine components to gas temperatures far greater than the softening temperatures of the nickel superalloys used to produce them. Ensuring sufficient component life in these conditions requires ever more effective cooling systems, which are fed by air being drawn away from the core compressor flow. The use of cooling systems in this manner thus limits the total power output of an engine. Additionally, coolant air must be discharged back into the mainstream flow, causing mixing losses and reducing aerodynamic efficiency. As such, it is crucial to design cooling systems that minimise the amount of coolant air used whilst accomplishing sufficient levels of cooling. One such cooling system that is well suited to meeting these goals is Double-Wall Effusion Cooling, which combines impingement, pin-fin, and effusion cooling to produce a high convective cooling efficiency (1) and overall cooling effectiveness (2). Said systems have been researched for some time, but applications have been limited by manufacturing difficulties and high thermomechanical stresses. An example of a Double-Wall Effusion Cooled NGV is shown in Figure 1.

$$\eta_{conv} = \frac{T_{c,e} - T_{c,i}}{T_{m,ave} - T_{c,i}} \tag{1}$$

$$\varepsilon_o = \frac{T_\infty - T_{m,ave}}{T_\infty - T_{c,i}} \tag{2}$$

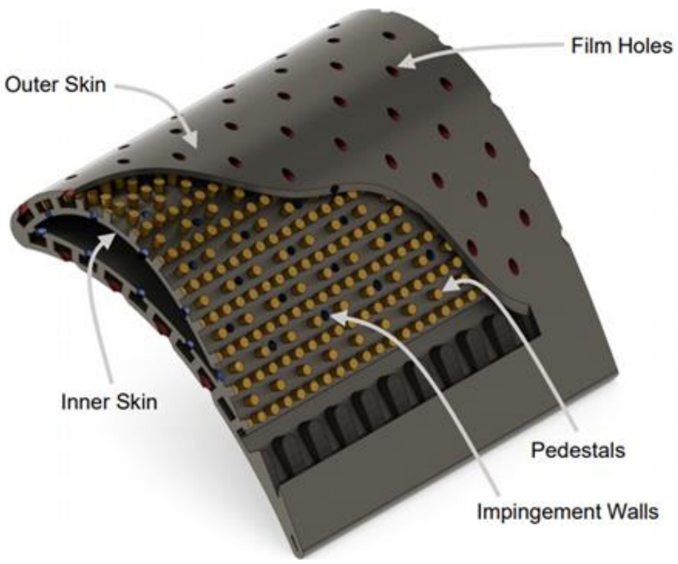

Figure 1: Turbine Blade using Double-Wall Effusion Cooling Scheme [1]

Whilst the design of Double-Wall Effusion Cooling systems has been increasingly well covered in the literature, the performance of said systems under standard manufacturing variability has not been the subject of extensive research, nor is there literature on how their tolerances may be optimised to reduce manufacturing cost. This paper sets out to address these issues through the use of a Low Order Flow Network Model (LOM) that has previously been developed and validated experimentally [2]. Firstly, the individual effects of select key geometric parameters on the cooling performance and coolant usage are quantified within standard manufacturing variations. These are combined in a Monte Carlo statistical analysis to review the likelihood and magnitude of full-blade performance variations. Finally, a multi-objective optimisation study is conducted to maximise the manufacturing tolerances (and thus minimise cost) and minimise coolant usage of a Double-Wall Effusion cooled NGV.

2 Related Work

2.1 Double-Wall Effusion Cooling Systems

A breadth of literature is available on the three component cooling systems that make up Double-Wall Effusion Cooling systems, all of which are well understood. Bunker [3] referred to Double-Wall cooling as “transpiration-like”, as these cooling systems look to move cooling mechanisms closer to the source of heat in a manner akin to transpiration whilst avoiding the strength and manufacturing issues associated with the extremely high porosity of transpiration cooling. Bunker estimated that Double-

Wall hybrid cooling systems may reduce coolant flow rates by 15-20% from the current state of the art in turbines.

Recently, the combined systems were studied computationally by Murray et al. [1], who conducted a parameter-based analysis of how geometries affected cooling performance and thermomechanical stresses – it was observed that designs which improved overall cooling often adversely affected thermomechanical performance.

Courtis & Ireland [4] conducted a similar computational study for significantly higher-porosity outer skins, noting that such designs led to impingement cooling being replaced as the dominant cooling mechanism by in-effusion hole cooling. Compared to less porous designs both the aerothermal and thermomechanical performances were improved, but at an increased risk of hot gas ingestion (indicated by a low Backflow Margin (3)). Wambersie et al. [5] tested similar high-porosity outer skins experimentally and demonstrated that such panels could achieve very high film effectiveness (>95%) even for low coolant mass flow rates.

$$BFM = \frac{P_{f,in,0}}{P_{f,e}} \tag{3}$$

2.2 Effect of Manufacturing Tolerances

The effects of manufacturing tolerances on turbine cooling have been the focus of several studies in the literature over the last 15 years – this paper predominantly looks to build from the work of two publications in particular. The first, by Bunker [6], used a simplified cooled aerofoil model to investigate the effects of a large number of manufacturing tolerances on the metal cooling effectiveness and coolant flow rate. The individual effect of each factor was examined by calculating the change in maximum metal temperature over the tolerable range of said parameter, where the maximum metal temperature was able to rise by nearly 40 K at engine conditions due to changes in the film hole diameter and impingement hole array spacing. The probability of such changes was then assessed through a 20,000 sample Monte Carlo statistical analysis – the range of temperature change was ±20 K, with 13.5% of them having a flow rate deviation greater than ±5%, which would lead to a significant number of parts being rejected. This paper emphasised the need for greater understanding of the effects of tolerances which were not meeting the performance metrics required at a sufficient rate.

The second key publication to this study was done by Dow & Wang [7], in which a computational test was conducted to simultaneously optimise a compressor blade geometry for minimised mean total pressure loss and maximised manufacturing tolerances. In multiple application cases, two optimised geometries were produced – a 'Deterministic' geometry where the nominal design performance was optimised alone, and a 'Tolerance' geometry optimised for the two simultaneous goals described. For a subsonic case, both geometries had better design-point performances than a baseline geometry, with the Deterministic being slightly better. When variations due to manufacturing tolerances were applied, however, the Tolerance design experienced much less drop off, with the mean performance only 1% worse than the design performance – the Deterministic geometry suffered a 6% drop off whilst subject to standard manufacturing tolerances. The optimised tolerances of the Tolerance geometry also reduced manufacturing cost, with the associated cost function being 49% lower than for the baseline case.

Other studies have focused on reviewing the performance of true-scale manufactured parts, complete with standard manufacturing variability. Knisely et al. [8] tested nine such test pieces experimentally, using IR thermography to capture the thermal performance. Correlating the cooling effectiveness to blade life, the authors estimated that "the hottest blade would be expected to survive only 47% as long as the coolest blade", showing the major effect of geometric variations within their manufacturing tolerances. Lee et al. [9] obtained 3D scans of 294 HPT rotor blades "taken from manufacturing line of an aero-engine company". These scans were processed to be tested computationally, where manufacturing variations "caused the shock to move forward of the design intent location", allowing the boundary layer to diffuse over a greater length of the blade, leading to a greater boundary layer momentum thickness (up by 13.5% on the SS).

Camci & Arts [10] reviewed the effects of flow incidence for a turbine blade, varying from -10° to +15°. Varying incidence resulted in the location of the stagnation point to change, resulting in significant changes to the external heat load and showerhead coolant distribution for the front 30% of the blade. More recently, Benabed et al. [11] conducted a computational investigation on the effects of incidence from -10° to +10° at several blowing ratios. At a high blowing ratio (M = 1.5) and low incidence, the SS film coolant jet was seen to penetrate far enough into the mainstream such that it was inverted onto the Pressure Surface, leaving the Suction Surface completely unprotected. However, the authors concluded that the overall influence of incidence angle variation in this range can be regarded as “small”.

Several studies have focused on the effects of manufacturing tolerances on film cooling effectiveness. Lee et al. [12] performed an optimisation study of a film cooling array whilst accounting for variations in performance due to manufacturing variations – as such, a multi-objective study was conducted, aiming to maximise the mean cooling effectiveness and minimise its variation with standard manufacturing variations. Compared to a baseline case, these goals were improved by 7.66% and 62.53% respectively. Kang et al. [13] reviewed potential in-tolerance misalignments of laidback fan-shaped film holes, finding that misalignments could have a severe effect on the level of diffusion accomplished – within tolerable variations, film cooling effectiveness could increase from the design case but could also fall by up to 70%.

Panizza et al. [14] estimated the probability of hot gas ingestion due to a low BFM using a rapid flow network tool and stochastic expansion methods. For a combined impingement and film cooling system, the BFM was shown to be most sensitive to the external static pressure, followed by the film hole and impingement hole diameters respectively. The pre-impingement total pressure and temperature had near-negligible influences.

3 Modelling Methodology

The Low Order Flow Network Model used for this study was fully presented and its experimental validation shown in [2], within which greater detail is available. In brief, flow networks simplify the flow’s paths and property changes into one-dimensional networks, made up of nodes which represent physical points in the system and links which represent the paths which connect them. Flow networks have been used in previous studies with considerable success (see [15, 16, 17, 18]).

The model used here combines two networks – 'The Continuity Network', which determines the coolant mass flow through the fluid domain by solving for static pressure at each node, and 'The Energy Network', which determines the energy transfer rates through both the fluid and solid domains by solving for static temperature at each node. The two networks, shown in Figure 2, are coupled and solved simultaneously using Newton's method. Mass and energy transfer rates along the links between any two nodes are determined by their pressure or temperature differences respectively, and their link's compliance to the transfer – this compliance is found from an empirical correlation, such as a discharge coefficient for mass flow through a cooling hole (all are listed in [2]). Film cooling effectiveness is found using a modified Goldstein correlation [19] with Sellers' superposition method [20]. All combined, the correlations are valid for internal flow Re values of 10^4 to 3×10^4. Coolant flow is assumed to be steady and incompressible along each link, whilst inlet and mainstream conditions remain fixed.

For this study, the model is applied to a full vane NGV, based on that tested by Holgate et al. [21] – external pressure and velocity distributions were obtained from this study. The external HTC distribution was calculated using the Ambrok method [22] as explained by Kays & Crawford [23].

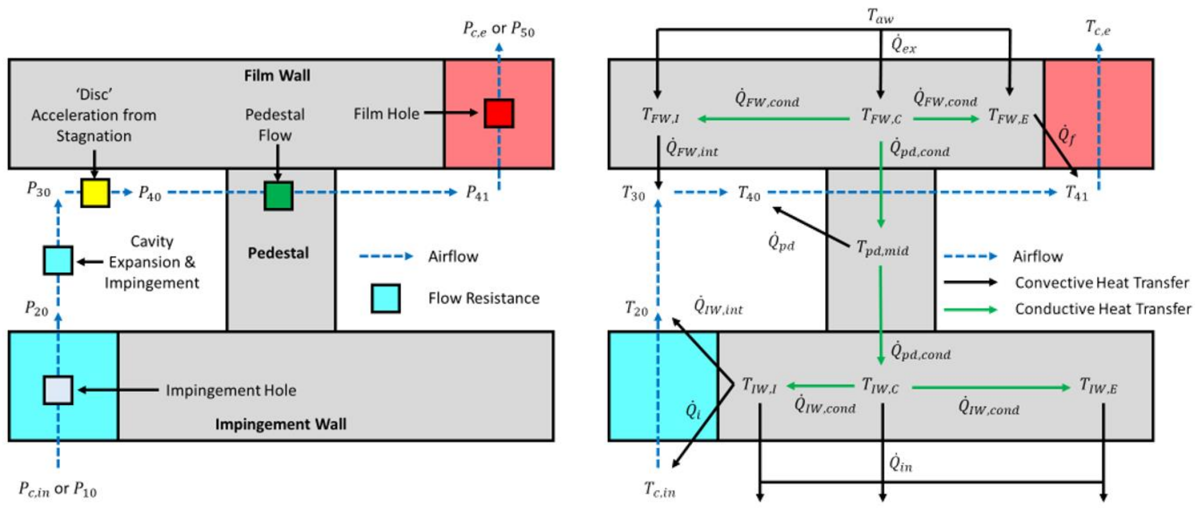

Figure 2: Diagrams of (a) The Continuity Network and (b) The Energy Network

Coolant supply conditions were chosen to give an inlet pressure to mainstream stagnation pressure ratio of 1.03 and a mainstream-to-coolant temperature ratio of 2. The application to a full vane context is shown by the example results of Figure 3. A wall is used in the pedestal cavity at the early SS to prevent excessive coolant migration [24] , stopping internal crossflow in the region with the greatest external pressure gradient. Results for the energy network are shown in terms of the external metal cooling effectiveness (4). The Trailing Edge of the vane is not included. The scheme tested, which keeps the array formation of Figure 1, has 30 impingement holes, 30 effusion holes, and 245 pedestals.

$$\boldsymbol{\eta_m} = \frac{\boldsymbol{T_\infty - T_{m,max}}}{\boldsymbol{T_\infty - T_{c,i}}} \tag{4}$$

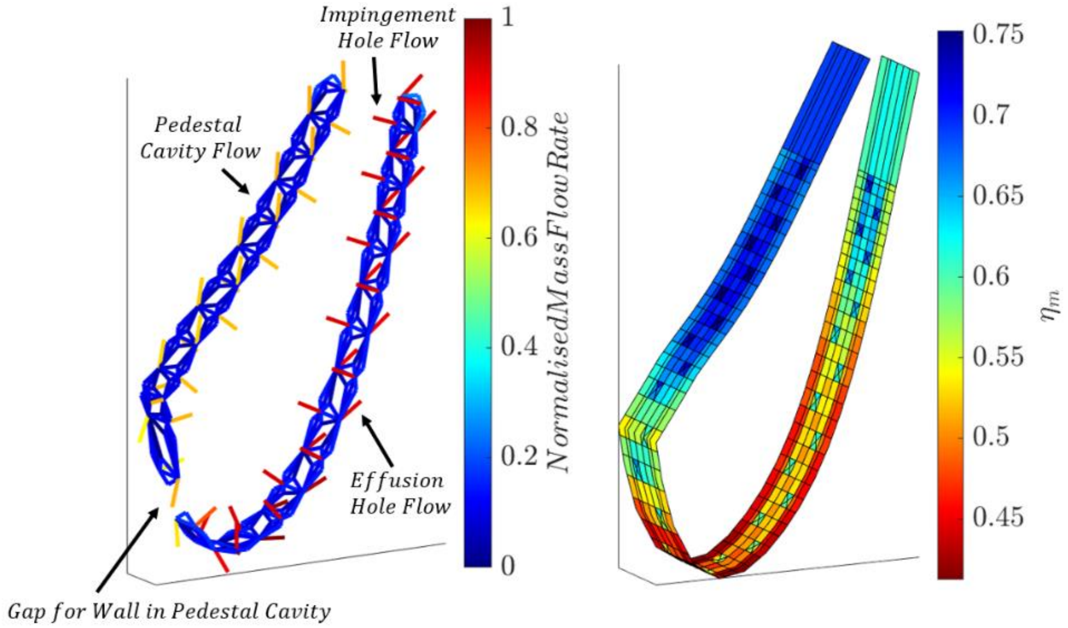

Figure 3: Baseline Results for (a) The Continuity Network and (b) The Energy Network

4 Geometric Parameters & Tolerances

The geometric parameters to be investigated, as well as their nominal values and standard tolerances, are listed in Table 1. Where possible, values for tolerances are taken from those used by Bunker [6]. For all geometries unless specified, the same manufacturing variation applies to all features of the same type. Hole spacings are the same for the inner and outer skins, with the zero position being set at the Stagnation Line – when streamwise spacing is varied, the row of holes at the Leading Edge does not move whilst those closest to the Trailing Edge will be most affected. The total outer surface area of the vane and the numbers of each geometric feature remain constant for all manufacturing variations. The baseline's (Geometry B) design performance metrics are listed in Table 2. It should be noted that this study does not include or consider the effects of a Thermal Barrier Coating on the vane's surface.

Parameter	Nominal Value	Tolerance
Impingement Hole Diameter d_i	0.5 mm	±10%
Effusion Hole Diameter d_f	0.5 mm	±10%
Pedestal Diameter d_{pd}	0.5 mm	±20%
Impingement Wall Thickness t_i	1.0 mm	±10%
Effusion Wall Thickness t_f	1.0 mm	±10%
Pedestal Height h_{pd}	1.0 mm	±20%
Hole Spanwise Spacing s_{span}	5.0 mm	±10%
Hole Streamwise Spacing s_{stream}	5.0 mm	±10%
Film Hole Inclination α_f	30°	±10°

Table 1: Baseline Geometric Parameters with nominal values and tolerances

$\frac{\dot{m}_c}{\dot{m}_{c,0}}$	η_m	BFM
1	0.4148	1.0194

Table 2: Baseline Geometry Performance

5 Results & Discussion

5.1 Effects of Geometric Parameters

In the first set of tests, the effect of each geometric parameter was assessed by varying it for its entire tolerance range whilst keeping all other parameters at their nominal value. Results for the changes in the maximum metal temperature, flow rate and Backflow Margin are shown in Figure 4.

The results of Figure 4(a) show how each parameter's variance can affect the maximum surface temperature. The hot spot where this temperature appeared was consistent – at the edge of the early SS where the heat load is greatest. At this location, there is only solid – heat must be conducted away to non-local internal cooling mechanisms. Additionally, the local film cooling is relatively poor due to films not yet being able to build up. This leads to the most crucial parameter being the streamwise spacing – low spacing means a high density of cooling features around the early SS, leading to a reduction in the maximum temperature of 17 K from the baseline. At the high end of this tolerance, high spacing reduces the density of cooling features and causes the maximum temperature to rise by 21 K from the baseline value – a total spread of 38 K. The closeness of the cooling features to the edge is controlled by the spanwise spacing, leading it to have a similar (if somewhat reduced) influence.

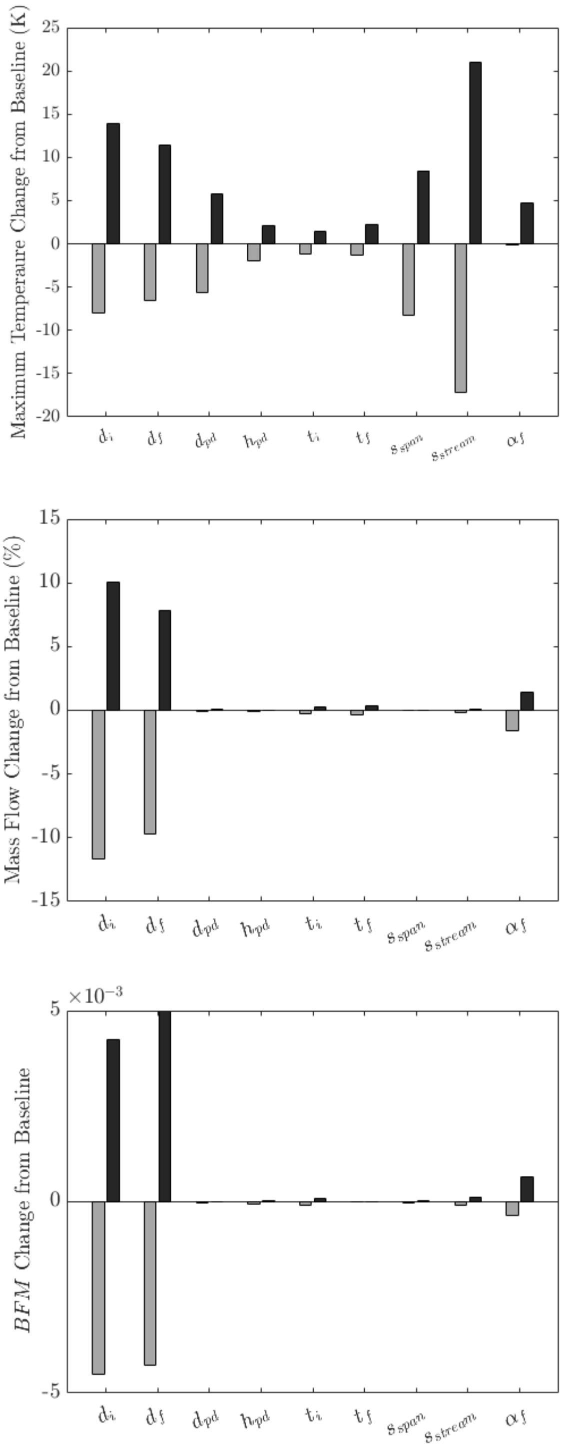

Figure 4: Maximum Positive (Grey) and Negative (Black) changes to (a) Maximum Temperature (b) Coolant Flow Rate & (c) Backflow Margin due to Parameter variance within tolerance range

Outside of spacing concerns, major variations in metal temperature are seen by variations in the cooling features – the influence of impingement hole diameter is greater than that of the effusion hole diameter due to the poor film cooling in the region of greatest heat load. Pedestal cooling increases as the pedestal surface area increases, but less benefit is acquired when raising height rather than diameter as a high pedestal height lessens the impingement jet Nu. The spread in maximum temperatures due to variations of the pedestal diameter and height are widened by the higher design tolerance of 20%.

Both the coolant mass flow (Figure 4(b)) and BFM (Figure 4(c)) variations are controlled nearly exclusively by the hole diameters – these are the effective throats of the cooling system and the porosity ratio between the outer and inner walls determines the share of pressure losses throughout the system. The effusion hole inclination does have a non-negligible effect on both $\dot{m}_c$ and BFM as it has a major influence of the effusion holes' discharge coefficients.

5.2 Full-Vane Monte Carlo Analysis

To assess the likelihood of the extreme changes in performance from Section 5.1, a 1000 sample Monte Carlo simulation was performed. Each parameter was assumed to be normally distributed within the bounds of its tolerance (such that the tolerances equal three times the standard deviation of the parameter). Figure 5 shows the results of this simulation. As parameters could vary simultaneously, more extreme variations could be observed – the maximum temperature varied from approximately 24 K below the baseline to 28 K above it, whilst the coolant mass flow rate varied by over ±15%. These high variations could have severe consequences for the vane's life – 17.4% of cases had a maximum temperature at least 10 K greater than the baseline, which would generally be expected to half the component's creep life [25]. The maximum temperature deviation from the baseline had an average of +2 K and a standard deviation of 8.5K.

An additional 10% usage of coolant would drastically increase mixing losses as coolant enters the turbine's mainstream flow, reducing aerodynamic efficiency – the Monte Carlo analysis shows this would happen in 11.8% of cases. On average, the total mass flow was 0.22% lower than the baseline, with a standard deviation of 4.5% of the baseline flow. The lowest achieved BFM was 1.0127, not so much lower than the baseline as to raise major hot gas ingestion concerns.

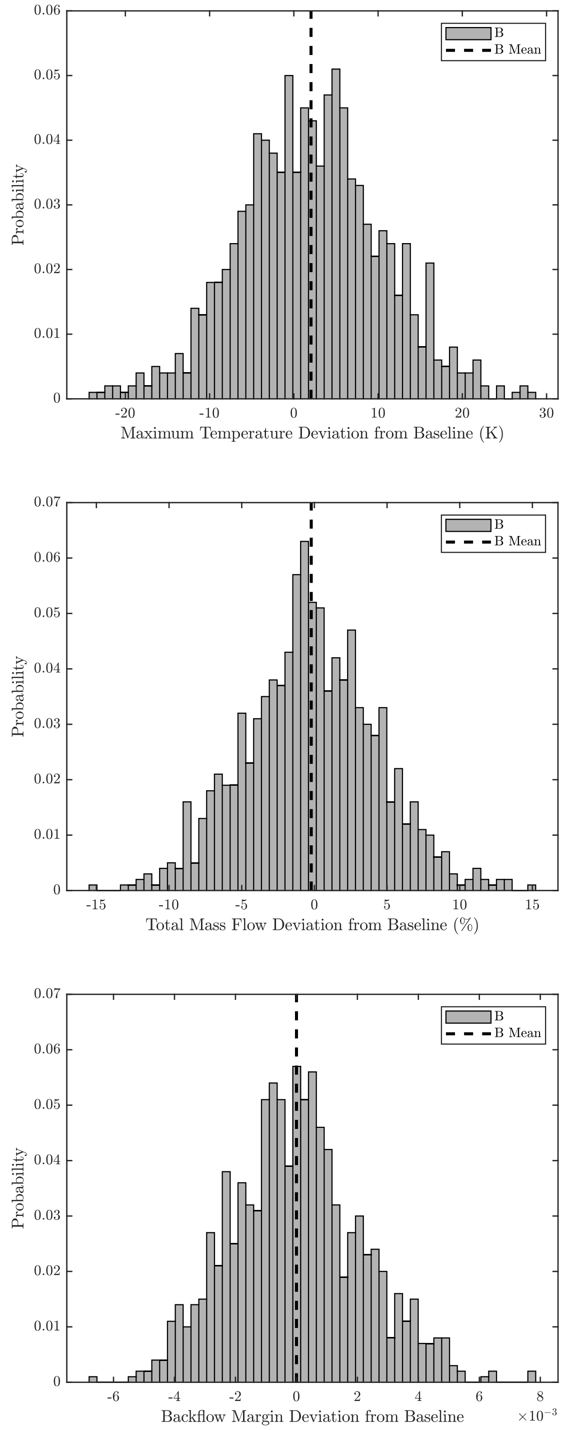

Figure 5: Monte Carlo Analysis results for (a) Maximum Temperature (b) Coolant Flow Rate & (c) Backflow Margin. Dashed Lines show Mean Performance.

An additional consideration to be made is that for some methods of manufacture, the quality of features such as holes and pedestals will not be identical around the vane (e.g. additive manufacturing where the feature orientation changes with respect to the build direction). To take this into account, a second Monte Carlo simulation was performed with the same number of samples, but in a case where the variations to hole and pedestal diameters were applied individually to each row. This meant that the likelihood of the most extreme circumstances – all effusion hole diameters being their smallest possible value, for example, was significantly reduced. The resulting performance distributions are shown in Figure 6. Immediately noticeable from Figure 6(b) is that the range of coolant mass flow variance is drastically reduced, with a range of -3.4% to +3.7% of the baseline flow rate, less than a quarter of the range when all diameters of a certain feature were equal. This is unsurprising, given how crucial the hole diameters are in setting the coolant mass flow (as shown by Figure 4(b)) – with the likelihood of all holes being on the edge of their tolerance range reduced, the potential for severe coolant flow rate change reduces. The mean coolant flow rate change from the baseline was +0.08%, with a standard deviation of 1.19%.

The effect on the Backflow Margin is similar, with the range of results falling to about a third of those from Figure 5(c). High variations in the BFM occur when the effusion-wall-to-impingement-wall porosity ratio moves away from unity – the lack of consistent hole sizes makes this less likely, reducing the chance of extreme BFM changes.

The same reduced range of effects is not observed for the maximum temperature change, shown in Figure 6(a). The range of temperature deviations is of similar size to Figure 5(a), now from -25 K to +26 K, but the probability of the maximum temperature being more than 10 K hotter than the baseline was reduced from 17.4% to 11.8%. The reason for this similar range is that the maximum temperature of the vane is very much a localised property, consistently occurring at the edge of the early SS. Regardless of the local effusion hole diameters, the region does not receive adequate effusion cooling due to a lack of build-up, and the temperature build up is in large part a function of how far removed internal cooling features are from this location – this is largely a product of the hole spacings s_{span} and s_{stream}, which do not have the same row variance and act as they did in the previous Monte Carlo study. The reduced risk of the higher temperatures, however, indicates that manufacturing each hole and pedestal independently reduces the risk of the 'perfect storm' conditions of high spacing and consistently small hole sizes that produces maximum temperatures more than 10 K higher than the baseline level. The mean temperature deviation was 1.44 K above the baseline, with a standard deviation of 7.3 K.

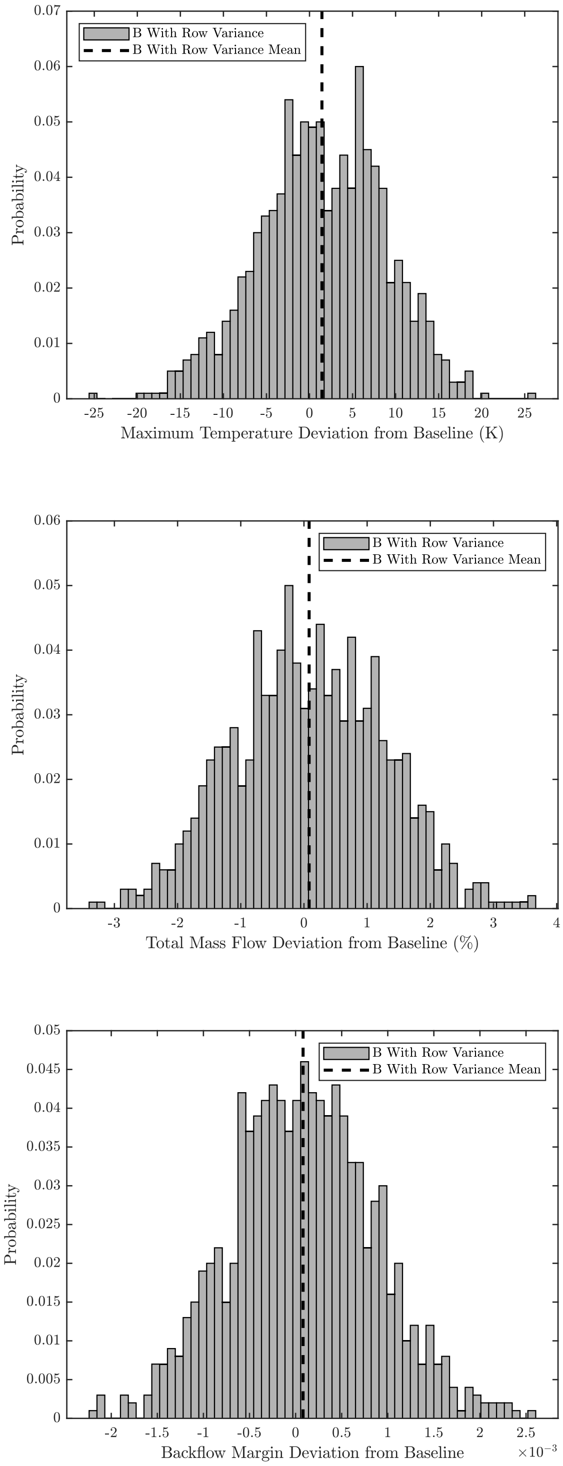

Figure 6: Monte Carlo Analysis results for (a) Maximum Temperature (b) Coolant Flow Rate & (c) Backflow Margin with Diameter Row Variance. Dashed Lines show Mean Performance.

5.3 Combined Performance & Tolerance Optimisation

The final set of tests performed in this paper was a combined performance and tolerance optimisation study. This aimed to produce a cooling system specification which minimised the use of coolant whilst achieving a minimum metal cooling effectiveness and sustaining an acceptable Backflow Margin for all effusion holes. This goal is summarised in (5). Furthermore, a second optimisation goal (6) was set to maximise manufacturing tolerances used, which would reduce the manufacturing cost. Geometries were tested at their design points and at two other specifications – based on results from Section 5.1, these were known to produce the lowest values of metal cooling effectiveness and Backflow Margin. For a geometry to be successful, the worst-case values of η_m and BFM had to be above a selected threshold.

$$\emptyset_{perf} = \frac{\dot{m}_{c,nom} - \dot{m}_{c,0}}{\dot{m}_{c,0}}$$

$$s.t.\ \eta_{m,min} > 0.4125 \tag{5}$$

$$\&\ BFM_{min} > 1.015$$

$$\emptyset_{tol} = \frac{W_{tol}}{\sum_p \sigma_p / \sigma_{0,p}} \tag{6}$$

W_{tol} is a weighting factor applied to the tolerance goal and $\sum_p \sigma_p / \sigma_{0,p}$ is the sum of the tolerances used normalised by their baseline values. The combined goal of the optimisation is summarised in (7).

$$\min\left(\emptyset_{perf} + \emptyset_{tol}\right) \tag{7}$$

The nominal values and tolerances of the 9 parameters listed in Table 1 were the design variables for this study. The acceptable ranges for their nominal values to vary in are listed in Table 3. Tolerances were accepted in the range 1-30%, such that no feature was able to be of a size to interfere with its neighbours. The upper bounds and tolerances for s_{span} and s_{stream} were limited to ensure that the number of hole rows remained the same for all geometries.

Parameter	Lower Bound	Upper Bound
d_i	0.25 mm	0.75 mm
d_f	0.25 mm	0.75 mm
d_{pd}	0.25 mm	0.75 mm
t_i	0.50 mm	1.50 mm
t_f	0.50 mm	1.50 mm
h_{pd}	0.50 mm	1.50 mm
s_{span}	3.50 mm	5.50 mm
s_{stream}	3.50 mm	5.50 mm
α_f	20°	50°

Table 3: Lower and Upper Bounds for Geometric parameters' nominal values

The optimisation was conducted using MATLAB's genetic algorithm software [26] – each generation had 50 designs, made up of 4 elites from the previous generation, 25 crossovers from previous designs, and 21 random 'mutated' designs. Convergence was found when the relative change in the combined goal was less than 10^{-3} over 10 generations.

For the benefit of comparison, 4 separate optimisation runs were carried out. Geometries T1, T2 and T3 had different values of W_{tol} (0.1, 1 and 10 respectively) to represent varying importance of manufacturing cost. A fourth deterministic geometry, D, was optimised for peak design performance alone, with manufacturing variations ignored and performances evaluated at the design point only. The final geometries for the four optimisation studies are listed in Table 4, and the design and mean performances of these four geometries as well as the baseline (Geometry B) are listed in Table 5. Mean performances were found through additional 1000 sample Monte Carlo simulations from the resulting tolerances. For the nominally-optimised Geometry D, mean performance values are assessed using the standard baseline tolerances as listed in Table 1.

The geometries produced from the optimisation algorithms are remarkably similar. All geometries seek a few features in particular, primarily small effusion hole diameters to act as the throat of the system and cap the total mass flow well below the baseline level per the $\emptyset_{perf}$ optimisation objective. Similarly, all geometries possess impingement hole diameters larger than the baseline – this reduces the pressure loss associated with the impingement process and guarantees that the BFM_{min} requirement is met. The high impingement hole diameter also makes up for some of the loss in cooling caused by reducing the effusion hole diameter. The small effusion holes lead to greater in-hole coolant velocities and thus higher blowing ratios, causing more jet lift-off and reducing film cooling effectiveness. This is demonstrated by the results of Figure 7, which compares the spanwise-averaged film cooling effectiveness for geometries B and D at their design points. For both geometries, low Pressure Surface mainstream velocities lead to complete jet-lift off. Yet whilst the baseline geometry sees a consistent build-up of films along the SS, the effect is much weaker for D.

Geometry	**D**	**T1**		**T2**		**T3**	
Parameter	Nom	Nom	Tol (%)	Nom	Tol (%)	Nom	Tol (%)
d_i	0.57	0.61	±1	0.75	±1	0.75	±30
d_f	0.28	0.29	±1	0.30	±1	0.32	±1
d_{pd}	0.75	0.72	±1	0.75	±1	0.70	±1
t_i	1.36	1.32	±30	1.31	±30	1.50	±30
t_f	1.40	1.37	±15	1.50	±30	1.46	±30
h_{pd}	1.48	1.45	±1	1.43	±1	1.50	±30
s_{span}	5.44	5.42	±3	5.38	±13	4.88	±30
s_{stream}	3.50	3.50	±1	3.50	±1	3.50	±1
α_f (˚)	20.0	20.0	±1	20.0	±1	21.5	±6

Table 4: Nominal Designs and Tolerances of Optimised Geometries – all in mm unless otherwise specified

Geometry	**Nominal**			**Mean**		
	$\frac{\dot{m}_c}{\dot{m}_{c,0}}$	η_m	BFM	$\frac{\dot{m}_c}{\dot{m}_{c,0}}$	η_m	BFM
B	1	0.415	1.0194	0.998	0.417	1.0194
D	0.442	0.413	1.0434	0.441	0.412	1.0432
T1	0.479	0.422	1.0436	0.478	0.422	1.0435
T2	0.521	0.431	1.0450	0.521	0.430	1.0448
T3	0.599	0.442	1.0445	0.597	0.441	1.0442

Table 5: Nominal and Mean Performance Results for optimised geometries

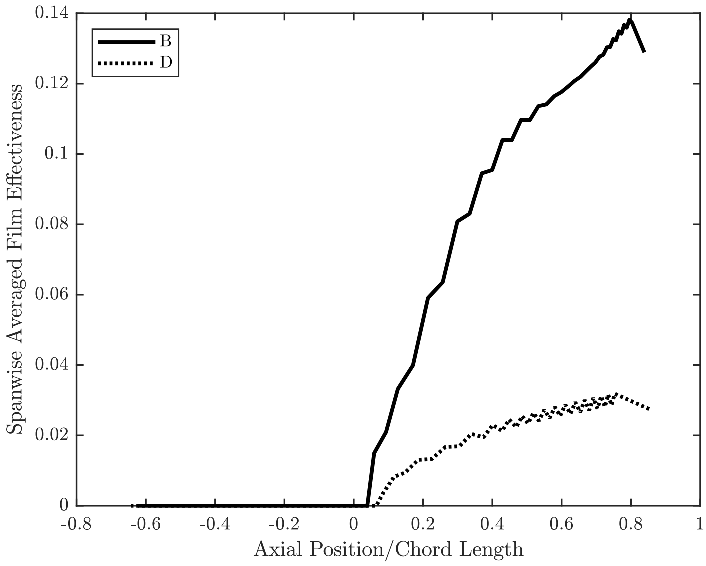

Figure 7: Axial Position vs. Spanwise averaged η_f. Negative Postion For Pressure Surface, Positive Position for Suction Surface

However, as has been noted previously, in this case study the main hot-spot at the edge of the early SS receives very little film cooling anyway, so reduced film cooling effectiveness does not meaningfully impact the minimum metal cooling effectiveness. Other consistent trends in the design include maximisation of the pedestal diameter, effusion wall thickness, and pedestal height. All three serve to maximise the surface area over which heat transfer can take place, allowing a reduction in coolant usage for the same cooling benefit. All geometries also sought a minimised effusion hole inclination – this increases the length of the effusion holes and thus their internal area, again enhancing the internal cooling effectiveness. The spanwise spacing of the holes is increased for all geometries, moving cooling features closer to the hot spot that emerges at the edge of the early SS. To target the same area, the streamwise spacing is minimised in all cases, keeping a high density of cooling features around the region with the hottest heat load. Figure 8, which compares B and D's respective metal cooling effectiveness variations with axial position, shows that there is only a small gap between the two around the early SS. This is despite D receiving far less coolant flow as its internal cooling has been optimised. Due to the low streamwise spacing, the Trailing Edge ends up much hotter for both surfaces on D compared to B.

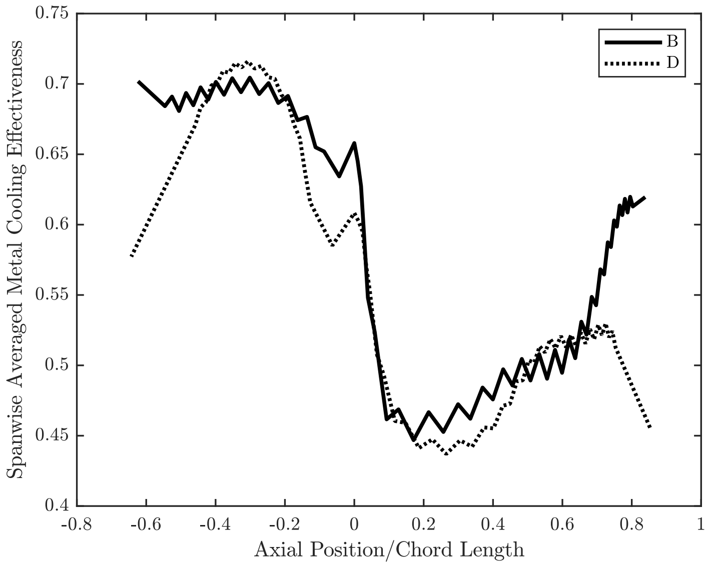

Figure 8: Axial Position vs. Spanwise averaged η_m. Negative Postion For Pressure Surface, Positive Position for Suction Surface

Turning now to a discussion of the optimised tolerances, one can see a general trend of the T geometries moving further away from geometry D as W_{tol} is increased, resulting in increasingly large design point mass flows. D, which accomplishes a design-point mass flow reduction of 55.8% but was never designed to compensate for any manufacturing variation, is unsustainable even with 1% tolerances applied. T1 can thus be viewed as a measure of how much the design point mass flow can actually be reduced whilst still meeting design criteria in its worst cases. With small tolerances applied to every geometric factor other than the two with the smallest impact on cooling performance (the wall thicknesses), T1's design point mass flow is 52.1% lower than the baseline (3.7% higher than D).

As the weighting toward increasing manufacturing tolerances increases, the optimisation algorithm has sought to increase tolerances primarily on the geometric parameters with lower impacts on the cooling performance. The most obvious example of this is the impingement wall thickness, which has very little effect on $\eta_{m,min}$ and can be varied without cost. The effusion wall thickness has only a small influence, as seen in Section 5.1, so can have a larger tolerance. For geometries T1 and T2, the only other variable with a non-minimal tolerance is the spanwise spacing – this runs slightly counterintuitive to the results of Section 5.1, where the spanwise spacing had a major influence on the cooling performance. The reason for the increased tolerance is the higher nominal cooling performance compared to the baseline geometry – deviations cause a drop off from a higher benchmark. The high nominal value of spanwise spacing limits the drop off in cooling performance at the narrowest allowed spacing. However, the larger tolerances for spanwise spacing and effusion wall thickness result in T2 needing a larger nominal coolant mass flow rate that is over 4% of the baseline rate higher than T1.

T3, which is designed to heavily favour high tolerances over nominal performance, has uniquely large tolerances for the impingement hole diameter and pedestal height. To compensate, the nominal mass flow rate is again increased, sitting at just under 60% of the baseline mass flow rate. The increased flow rate enables more flexibility – to allow for the impingement hole varying in diameter by 30%, the effusion hole size is increased to ensure that there is always enough coolant flowing through the system. The pedestal diameter is also slightly reduced, increasing the flow area through the pedestal array.

3 geometric parameters have minimal manufacturing tolerances throughout – the effusion hole diameter, the pedestal diameter, and the streamwise spacing. As the selected throat for each system, tolerances for the effusion hole diameter are kept low to prevent the holes becoming too small and limiting the coolant supply even further. The streamwise spacing is a special case – whilst the major hot spot at the edge of the early SS needed to be addressed, this could not happen at the expense of the rest of the vane. Larger tolerances could lead to cooling features being too far removed from the vicinity of the Trailing Edge, leading to a hot spot at the end of the vane that violated the $\eta_{m,min}$ requirement. Due to the small streamwise spacing required, pedestal diameters were not allowed large tolerances as there was insufficient space to fit them into the array. As the nominal values were maximised to increase their surface area, tolerances were minimised to prevent intersection.

Overall, the sum of the normalised tolerances $\sum_p \sigma_p/\sigma_{0,p}$ fell by 42% and 14% respectively for geometries T1 and T2 from the baseline value. For T3, it was increased by 55%. This indicates that a reasonably high weighting must be applied to increasing tolerances to prevent $\emptyset_{tol}$ from becoming lost behind $\emptyset_{perf}$. T3 is the only geometry where both the nominal performance (coolant usage) and manufacturing cost improved. Based on manufacturing requirements, different weightings could be applied to each parameter individually, likely leading to significantly different results. It is noted that for the effusion holes in particular, specifications of such small diameters with 1% tolerances are unfeasible for industry application – a higher weighting on said hole tolerance would likely avoid this result.

Figure 9 shows the results of the Monte Carlo analyses conducted for the three Tolerance-Optimised geometries. Immediately clear from Figure 9(b) and Figure 9(c), showing the variance in mass flow rate and Backflow Margin respectively, is the effect of the tighter tolerances placed on the hole diameters. The spread of mass flow rates compared to the baseline geometry (as seen in Figure 5) is much reduced, with both T1 and T2 having mass flow variances of less than 2.5% of the baseline mass flow. The Backflow Margins of these two geometries also remain tightly controlled. Geometry T3, which has an impingement hole diameter manufacturing tolerance much higher than the baseline, has a mass flow spread of less than 6% of the baseline mass flow – this is still smaller than the baseline variance due to the small tolerance allowed to the effusion hole diameter. Due to its high design value of the effusion wall to impingement wall porosity ratio, T3 does not come close to violating the BFM_{min} requirement.

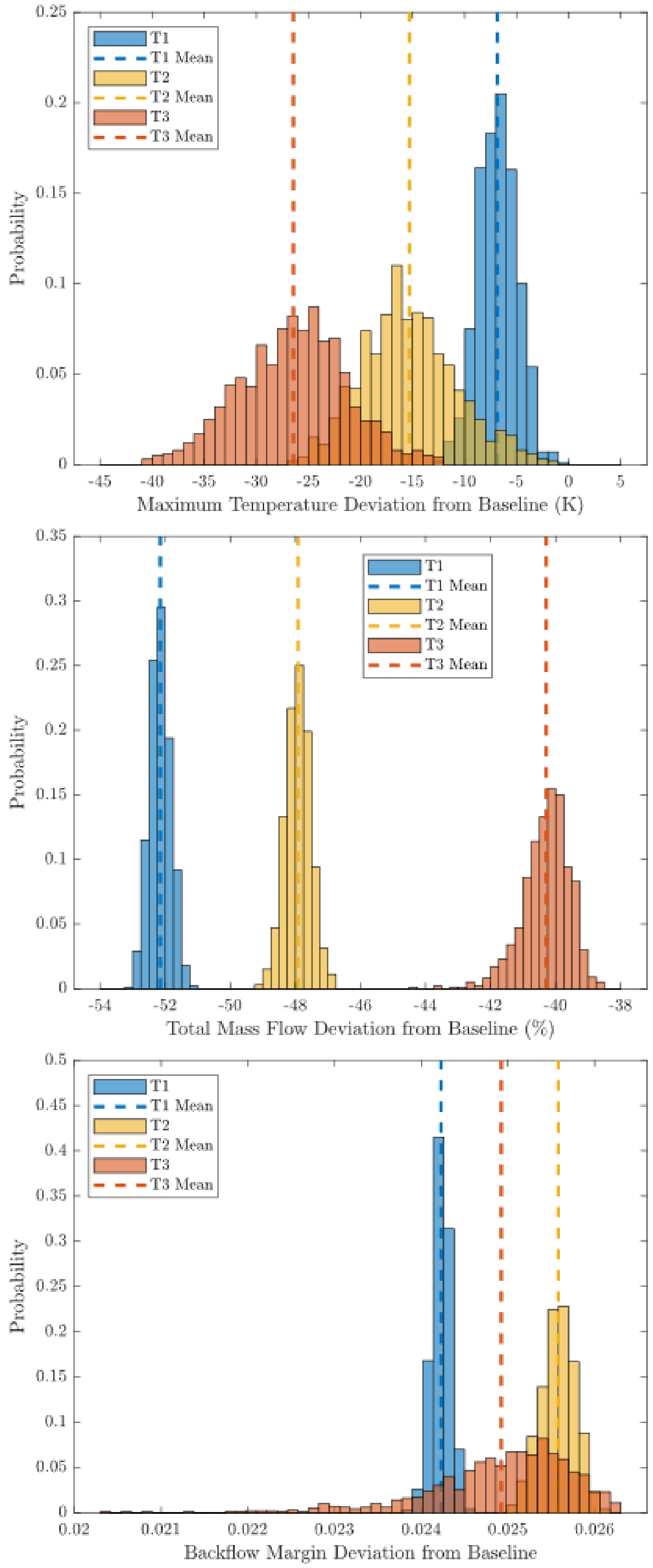

Figure 9: Monte Carlo Analysis Results for the 3 Tolerance-Optimised Geometries for (a) Maximum Temperature (b) Coolant Flow Rate & (c) Backflow Margin. Dashed Lines show Mean Performance.

Figure 9(a) essentially serves as a demonstration of how close each geometry comes to violating the minimum cooling requirement. As the baseline geometry achieved a nominal cooling effectiveness of 0.415, a maximum temperature deviation of +2.5 K would deem the design a failure. T1 appears to have some level of safety margin, with a maximum temperature deviation of -0.8 K. This indicates a potential for it to be pushed further in terms of minimising the total coolant mass flow – this could likely be accomplished by further lowering W_{tol} or by applying even stricter convergence criteria to the Genetic Algorithm optimisation process. T2 has a similar worst-case performance, with a maximum temperature deviation of -1.2 K. Due to its greater design hole diameters and higher coolant flow, T3 has a minimum metal cooling effectiveness of 0.427, still 12.5 K colder than the nominal baseline performance.

For comparison, the Monte Carlo analysis results for Geometry D are shown in Figure 10. It is obvious from these results that standard manufacturing tolerances cannot in practice be applied to a nominal performance-optimised geometry – the maximum temperature deviation from the baseline is over 42 K, equivalent to a metal cooling effectiveness of 0.373. This is primarily a result of the high coolant mass flow spread, which ranges from just below -64% to -48% of the baseline coolant mass flow. Such variation in coolant supply when the design point only just satisfies the $\eta_{m,min}$ requirement has predictable and dire consequences. The Backflow Margin's variance is less than that of T3, as each hole's diameter can vary only by 10% as opposed to T3's impingement hole's 30%. The poor performance of Geometry D when subject to manufacturing variations emphasises the benefit of considering and optimising the nominal values and tolerances of geometry parameters simultaneously when designing cooling systems.

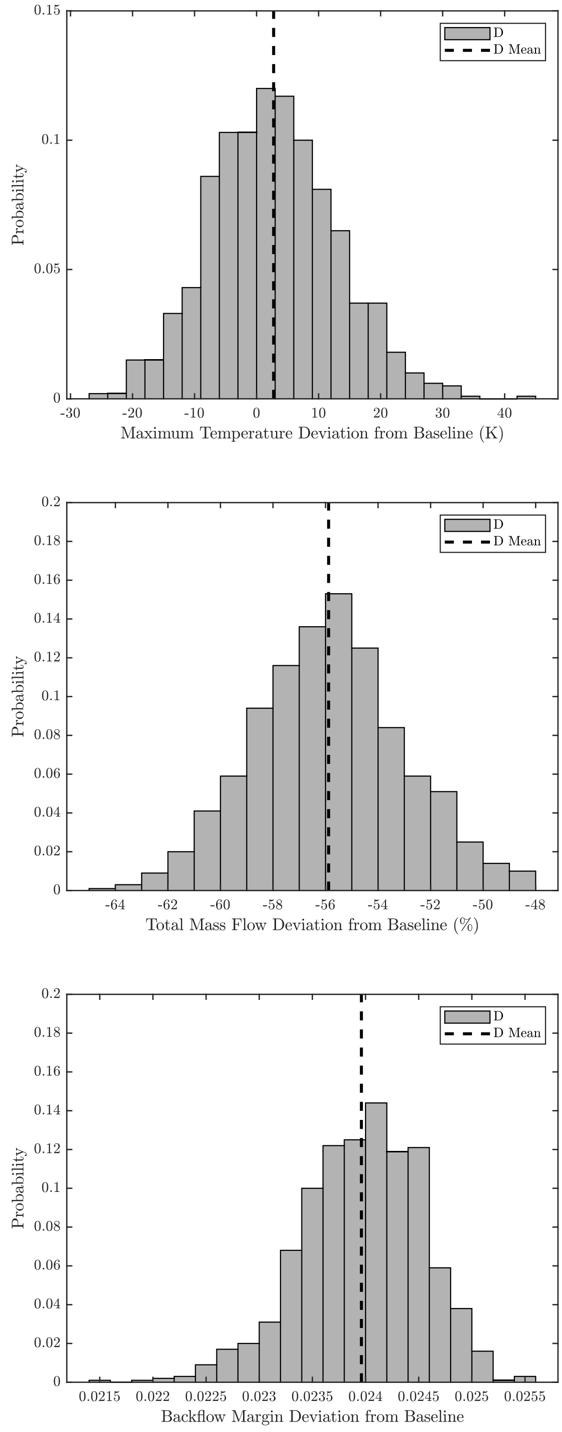

Figure 10: Monte Carlo Analysis Results for the Nominal Performance-Optimised Geometry D for (a) Maximum Temperature (b) Coolant Flow Rate & (c) Backflow Margin. Dashed Lines show Mean Performance.

6 Conclusion

A Low Order Flow Network Model has been used to investigate the effect of manufacturing tolerances on the performance of a Double-Wall Effusion Cooling System. This investigation has shown that for a standard baseline geometry, the maximum metal temperature and coolant flow rates can vary significantly within standard tolerances. Changes in flow rates were governed by hole diameters alone, whilst the maximum metal temperature was heavily influenced by both the hole diameters and the hole spacings. A Monte Carlo analysis was conducted to find the effect of multiple geometric variations at the same time. This showed that the performance of the cooling system was subject to major fluctuations, including rises in the maximum metal temperature of nearly 30 K and increases in coolant usage by over 15%. When hole and pedestal diameters were made to vary on a row-by-row basis, as if a separate tool was used to manufacture them rather than the same one throughout the vane, coolant usage fluctuations were much reduced, but the maximum metal temperature continued to be susceptible to high rises due to an exposed hot spot at the edge of the early SS. To review if such fluctuations could be eliminated whilst reducing the manufacturing cost and coolant usage, an optimisation study was conducted. This showed that it was possible to reduce both the design point coolant flow rate and the manufacturing cost simultaneously, but only when high weighting was given to maximising manufacturing tolerances.

Future work will look to account for the thermomechanical performance alongside the aerothermal performance of the vane. Research in the literature [27] suggests that achieving such high tolerances for the impingement wall thickness would be unlikely when component life is considered. Additionally, a view toward separating sections of the vane may allow region specific optimisation of tolerances – the low tolerances required at the Leading Edge and early Suction Surface are unlikely to be necessary in other areas such as the Pressure Surface, where tolerances could be relaxed and manufacturing cost reduced.

Acknowledgements

This work is supported by Rolls Royce plc. and the EPSRC under the CDT in Gas Turbine Aerodynamics (EP/L015943/1) and the Transpiration Cooling Systems for Jet Engine Turbines and Hypersonic Flight Programme Grant (EP/P000878/1).

Nomenclature

A	Area $\left(\boldsymbol{m^2}\right)$
BFM	Backflow Margin
d	Diameter $(\boldsymbol{m})$
h	Height $(\boldsymbol{m})$
$\dot{m}$	Mass Flow Rate $(\boldsymbol{kg/s})$
NGV	Nozzle Guide Vane
P	Pressure $(\boldsymbol{Pa})$
Re	Reynolds Number
s	Spacing $(\boldsymbol{m})$
SS	Suction Surface
t	Thickness $(\boldsymbol{m})$
T	Temperature $(\boldsymbol{K})$
TET	Turbine Entry Temperature
α	Inclination (°)
ε_o	Overall Cooling Effectiveness
η	Effectiveness or Efficiency
σ	Tolerance
ϕ	Objective
Subscripts	
0	Baseline or Total
ave	Average
aw	Adiabatic Wall
c	Coolant
$cond$	Conductive
$conv$	Convective
e or E	Exit
ex	Exterior
f	Film/Effusion
FW	Film/Effusion Wall
i or I	Impingement
int	Interior
in	Inlet
IW	Impingement Wall
max	Maximum
m	Metal
min	Minimum
nom	Nominal
p	Geometric Parameter
$perf$	Performance
pd	Pedestal
$span$	Spanwise
$stream$	Streamwise
tol	Tolerance
∞	Mainstream

References

[1] A. V. Murray, P. T. Ireland and A. J. Rawlinson, “An Integrated Conjugate Computational Approach for Evaluating the Aerothermal and Thermomechanical Performance of Double-Wall Effusion Cooled Systems,” in *ASME Turbo Expo 2017: Turbomachinery Technical Conference and Exposition*, Charlotte, North Carolina, 2017.

[2] M. van de Noort, A. V. Murray and P. T. Ireland, “Low Order Heat & Mass Flow Network Modelling for Quasi-Transpiration Cooling Systems,” Rotterdam, The Netherlands, 2022.

[3] R. S. Bunker, “Evolution of Turbine Cooling,” in *ASME Turbo Expo 2017: Turbomachinery Technical Conference and Exposition*, Charlotte, North Carolina, 2017.

[4] M. Courtis and P. T. Ireland, “Influence of Porosity on Double-Walled Effusion-Cooled Systems for Gas Turbine Blades,” Rotterdam, The Netherlands, 2022.

[5] A. Wambersie, H. Wong, P. T. Ireland and I. Mayo, “Experiments of Transpiration Cooling Inspired Panel Cooling on a Turbine Blade Yielding Film Effectiveness Levels over 95%,” *International Journal of Turbomachinery, Propulsion and Power*, vol. 6, no. 2, 2021.

[6] R. S. Bunker, “The Effects of Manufacturing Tolerances on Gas Turbine Cooling,” *ASME. J. Turbomach.,* vol. 131, no. 4, 2009.

[7] E. A. Dow and Q. Wang, “Simultaneous Robust Design and Tolerancing of Compressor Blades,” in *ASME Turbo Expo 2014: Turbine Technical Conference and Exposition*, Düsseldorf, Germany, 2014.

[8] B. Knisely, R. Berdanier, J. Wagner, K. Thole, A. Arisi and C. Haldeman, “Effects of Part-to-Part Flow Variations on Overall Effectiveenss and Life of Rotating Turbine Blades,” in *ASME Turbo Expo 2022*, Rotterdam, The Netherlands, 2022.

[9] W. Lee, W. Dawes, J. Coull and F. Goenaga, “The Impact of Manufacturing Variability on High Pressure Turbine Profile Loss,” in *AIAA Aerospace Sciences Meeting*, Kissimmee, Florida, 2018.

[10] C. Camci and T. Arts, “Effect of Incidence on Wall Heating Rates and Aerodynamics on a Film-Cooled Transonic Turbine Blade,” *ASME. J. Turbomach,* vol. 113, no. 3, p. 493–501, 1991.

[11] M. Benabed, A. Azzi and B. Jubran, “Numerical investigation of the influence of incidence angle on asymmetrical turbine blade model showerhead film cooling effectiveness,” *Heat and Mass Transfer,* vol. 46, pp. 811-819, 2010.

[12] S. Lee, D. Rhee and K. Yee, “Optimal Arrangement of the Film Cooling Holes Considering the Manufacturing Tolerance for High Pressure Turbine Nozzle,” in *ASME Turbo Expo 2016: Turbomachinery Technical Conference and Exposition*, Seoul, South Korea, 2016.

[13] Y. Kang, S. Park, J. Jeong, G. M. Kim and J. S. Kwak, “The effects of manufacturing tolerance on the film cooling effectiveness of a laidback fan-shaped hole,” *J Mech Sci Technol,* vol. 36, p. 2127–2137, 2022.

[14] A. Panizza, A. Bonini and L. Innocenti, “Uncertainty Quantification of Hot Gas Ingestion for a Gas Turbine Nozzle Using Polynomial Chaos,” in *ASME Turbo Expo 2015: Turbine Technical Conference and Exposition*, Montreal, Quebec, Canada, 2015.

[15] J. R. Rose, “NASA TM-73774: FLOWNET: A Computer Program for Calculating Secondary Flow Conditions in a Newtork of Turbomachinery,” NASA, Cleveland, Ohio, 1978.

[16] G. Ebenhoch and T. M. Speer, “Simulation of Cooling Systems in Gas Turbines,” in *ASME 1994 International Gas Turbine and Aeroengine Congress and Exposition*, The Hague, The Netherlands, 1994.

[17] H. Jin, A. Riddle and L. Cooke, “A Compressible Flow Network Analysis for Design Upgrade of Industrial Aeroderivative High Pressure Turbine Blades,” in *ASME Turbo Expo 2008: Power for Land, Sea, and Air*, Berlin, Germany, 2008.

[18] K. J. Kutz and T. M. Speer, “Simulation of the Secondary Air System of Aero Engines,” in *ASME 1992 International Gas Turbine and Aeroengine Congress and Expostion*, Cologne, Germany, 1992.

[19] R. J. Goldstein, “Film Cooling,” *Advances in Heat Transfer,* vol. 7, pp. 321-379, 1971.

[20] J. P. Sellers, “Gaseous Film Cooling With Multiple Ejection Stations,” *AIAA J.,* vol. 1, no. 9, pp. 2154-2156, 1963.

[21] N. E. Holgate, I. Cresci, P. T. Ireland and A. Rawlinson, “Prediction and Augmentation of Nozzle Guide Vane Film Cooling Hole Pressure Margin,” in *12th European Conference on Turbomachinery Fluid dynamics & Thermodynamics*, Stockholm, Sweden, 2017.

[22] G. S. Ambrok, “Approximate solution of equations for the thermal boundary layer with variations in boundary layer structure,” *Soviet Physics-Technical Physics,* vol. 2, no. 9, pp. 1979-1986, 1957.

[23] W. M. Kays and M. E. Crawford, Convective Heat and Mass Transfer, New York: McGraw-Hill, 1980.

[24] M. van de Noort and P. T. Ireland, “A Low Order Flow Network Model for Double-Wall Effusion Cooling Systems,” *International Journal of Turbomachinery, Propulsion and Power,* vol. 7, no. 1, 2022.

[25] G. F. Harrison, in *European Propulsion Forum, Royal Aeronautical Society*, London, 1993.

[26] MathWorks, “How the Genetic Algorithm Works,” 2022. [Online]. Available: https://uk.mathworks.com/help/gads/how-the-genetic-algorithm-works.html. [Accessed 7 April 2022].

[27] C. Skamniotis, M. Courtis and A. C. F. Cocks, “Multiscale analysis of thermomechanical stresses in double wall transpiration cooling systems for gas turbine blades,” *International Journal of Mechanical Sciences,* vol. 207, 2021.

